Eur. Phys. J. D **18**, 301–307 (2002)
DOI: 10.1140/epjd/e20020034

THE EUROPEAN PHYSICAL JOURNAL D
EDP Sciences

Dynamics of ionization mechanisms in relativistic collisions involving heavy and highly-charged ions

D.C. Ionescu and A. Belkacem

[1] Lawrence Berkeley Laboratory, University of California at Berkeley, M.S. 71-259, 1 Cyclotron Rd., Berkeley, CA 94720, USA
[2] Division of Physics, Gesellschaft für Schwerionenforschung, Planckstr. 1, 64291 Darmstadt, Germany
[3] Institut für Theoretische Physik, Technische Universität Dresden, Mommsenstr. 13, 01062 Dresden, Germany

Received 26 June 2001 and Received in final form 27 November 2001

Abstract. The dynamics of mechanisms associated with the ionization of inner-shell electrons in relativistic collisions involving heavy and highly-charged ions is investigated within a nonperturbative approach formulated explicitly in the time domain. The theoretical treatment is based on the exact numerical solution of the time dependent Dirac equation for two Coulomb centers on a lattice in momentum space. We present results for ionization in encounters between 100 MeV/u Au^{79+} projectile ions impinging on a hydrogen-like uranium target. By directly visualizing the collision dynamics we identify a new ionization mechanism in which electrons are emitted from the internuclear region preferentially in the transverse direction with respect to the projectile trajectory. A striking characteristic of this ionization mechanism is that the velocity of the electron is higher than the projectile velocity.

PACS. 34.50.Fa Electronic excitation and ionization of atoms (including beam-foil excitation and ionization) – 34.10.+x General theories and models of atomic and molecular collisions and interactions (including statistical theories, transition state, stochastic and trajectory models, etc.)

1 Introduction

Recent developments in the construction of accelerators for relativistic heavy ions opened new frontiers in atomic collision physics, and we are now in a position to extend our basic understanding of elementary atomic processes such as excitation, ionization, charge transfer and pair production in a wide range of energies and charges. A wealth of collision phenomena can be investigated both theoretically and experimentally in encounters involving heavy and highly-charged projectile ions with nuclear charge numbers up to $Z = 92$ and energies ranging from several tens of MeV/u upward.

Time-dependent perturbation theory in lowest order with a set of atomic basis states located at the position of the target generally provides a good description of ionization in the relativistic energy regime for small projectile charge numbers even for the heaviest targets. In encounters involving highly-charged heavy projectile and target ions, however, the situation is fundamentally different. Interactions involving high-Z ions in relativistic motion can become very strong due on one hand to the large value of the coupling constant $\alpha Z \geq 0.5$ (here, $\alpha \simeq 1/137$ is the Sommerfeld fine structure constant) and on the other hand to the enhancement of the transverse components of the electromagnetic field associated with the moving ions by the Lorentz factor γ. Under such extreme conditions large portions of the two center continuum are strongly distorted, and the momenta of ejected electrons can be quite high. As a result, perturbative calculations of impact-parameter dependent probabilities for ionization yield results which may become larger than one violating unitarity bounds [1–3].

Previous investigations in slow ion-atom collisions have identified two major mechanisms for ionization. In low-energy encounters electrons can either be promoted to the continuum through multistep transitions in the quasi-molecule formed during the collision (S mechanism), or they are picked up in the saddle region of the two-center potential surface and ejected to the continuum as the collision partners recede from each other (T mechanism) [4–6]. The relative importance of the different ionization mechanisms has been investigated in several experimental studies [7–10].

In the present work we show that in relativistic encounters involving high-Z collision partners the acceleration of the active electron may become quite high resulting in a new ionization mechanism. This mechanism is responsible for the emission of high velocity electrons from the internuclear region, well after the time of closest approach, preferentially in the transverse direction with respect to the beam axis. This behavior is distinctly different from the saddle point ionization mechanism known from slow atomic collisions where electrons are promoted with a relatively low velocity in the rest frame of the saddle point. This acceleration of emitted electrons to high energies is similar to the "Fermi-shuttle" acceleration

discussed in recently reported measurements [11] of electron emission to the continuum in ion-atom collisions at energies around 45 MeV/u. The velocity spectra obtained in [11] exhibit for targets as heavy as Au an unexpectedly large number of very fast electrons such that electrons with velocities considerable *higher* than the projectile velocity can be emitted as a result of multiple collision sequences. This multiple scattering mechanism also named "Fermi-shuttle" mechanism, where the active electron scatters several times in the two-center potential associated with the target and the projectile before its liberation to the continuum was invoked to explain high energy cosmic rays [12,13], anomalous fusion cross-sections in atomic cluster collisions [14,15], and also to account for fast electron emission in ion-atom collisions [11,16].

Due to recent advances in the development of high performance parallel computers, nonperturbative *ab initio* investigations of atomic collisions within the framework of the Dirac [17,18] or the Schrödinger equation [19,20] became feasible. In the present investigation we extend the study of the dynamics of ionization mechanisms to very strong-field conditions by investigating the collision between a 100 MeV/u Au^{79+} projectile ion impinging on a hydrogen-like uranium target. The present nonperturbative approach provides complete images in real-time of the probability density associated with the time-evolved wave function, enabling the direct investigation of specific features of the momentum distribution of an initially bound target electron as the collision evolves in time. In some sense, this method constitutes a theoretical complement to the new experimental imaging techniques using COLTRIMS [9,10] in that it provides a direct and complete visualization of the collision dynamics. Since the main nonperturbative features of excitation mechanisms are expected to occur at small internuclear separations where the electron experiences the maximum strength of the two-center potential associated with target and projectile, we report for simplicity only calculations for vanishing impact parameters. We do not expect this choice to change the main results and the conclusions of the present investigation. We use natural relativistic units ($\hbar = m = c = 1$) unless stated otherwise. As a result, energies are measured in units of the electron rest mass $mc^2 \simeq 511$ keV, lengths are measured in units of the reduced electron Compton wavelength $\lambda_C = \hbar/(mc) \simeq 386.16$ fm, and time is measured in units of the reduced Compton time $\tau_C = \lambda_C/c \simeq 1.29 \times 10^{-21}$ s.

2 Theoretical approach

Our approach is based on the time-dependent Dirac equation for one electron in the field of two Coulomb centers formulated in momentum space

$$\mathrm{i}\frac{\partial}{\partial t}\psi(\mathbf{k},t) = \left(\hat{\alpha}\cdot\mathbf{k} + \hat{\beta}\right)\psi(\mathbf{k},t) - \frac{\alpha}{2\pi}\int \mathrm{d}^3k' \left[\frac{Z_T}{q^2} + \frac{Z_P(1-v\hat{\alpha}_z)\mathrm{e}^{\mathrm{i}\mathbf{q}\cdot\mathbf{R}(t)}}{q_x^2+q_y^2+q_z^2/\gamma^2}\right]\psi(\mathbf{k}',t), \quad (1)$$

with the initial condition

$$\lim_{t\to-\infty}\psi_j(\mathbf{k},t) = \varphi_j(\mathbf{k})\,\mathrm{e}^{-\mathrm{i}E_jt}, \quad (2)$$

where the initial-state wave function φ_j is associated with an inner-shell, say, a target K-shell electron with energy E_j. In equation (1) the vector $\mathbf{q} = \mathbf{k} - \mathbf{k}'$ represents the momentum transfer, $\hat{\alpha}_z$ is the Dirac matrix in the z-direction, and $\gamma = \left(1-(v/c)^2\right)^{-1/2}$ is the relativistic Lorentz factor. The origin of the coordinate system is chosen to be at the center of the target nucleus with charge number Z_T. The projectile ion, with charge number Z_P, moves with constant velocity $\mathbf{v} = (0,0,v)$ at an impact parameter b parallel to the z-axis such that the internuclear distance $\mathbf{R} = (b,0,vt)$, and for the case of central collisions considered here one has $b = 0$. Thus, the xz-plane is the scattering plane, and for heavy ions in relativistic motion recoil and Coulomb deflection effects are neglected [21]. It is important to note that even at relatively low relativistic energies around 100 MeV/u ($\beta = v/c \simeq 0.4$ is *lower* than the nonrelativistic velocity $v_{1s} = \sqrt{2E_{\mathrm{kin}}/m} = \alpha Z \simeq 0.6c$ of a $1s$-electron in uranium as given by the Virial theorem, $E_{\mathrm{kin}} = E_B$, E_{kin} denoting the kinetic electron energy and $E_B = (\alpha Z)^2/2$ being its binding energy) magnetic effects are of considerable importance such that the complete Liénard-Wiechert interaction is incorporated in the integral kernel on the right hand side of equation (1). In [22] it is explicitly shown that for electronic excitations in this energy regime interferences between the different components associated with the Liénard-Wiechert interaction lead to up to a 30% reduction of cross sections demonstrating the importance of the magnetic interaction term proportional to $v\hat{\alpha}_z$ in equation (1).

In the numerical analysis of the integro-differential equation (1) we enclose the collision system in a finite volume in momentum space. In contrast to grid methods in configuration space where the boundary conditions are not fulfilled for realistic grid sizes due to continuum components of the wave function associated with ionization and charge exchange that spread over the entire space, in momentum space the wave function is confined to a finite volume and stays localized around the origin at all times. Thus, the momentum-space wave function is negligible small at the boundaries of the discretization volume used in practical calculations making momentum-space grid methods particularly well suited for numerical investigations of time-dependent wave equations. On the other hand, a general drawback of these numerically exact lattice approaches is that they are computationally very intensive.

In the present investigation we use massively parallel processing on the 640 processor Cray-T3E supercomputer of the National Energy Research Scientific Computing Center (NERSC) in Berkeley. Equation (1) is rewritten as a linear system of coupled equations which are integrated by a fourth-order Zonneveld-Adams-Moulton predictor-corrector method in the PECE scheme. The typical size of time step used in the integration routine is of the order

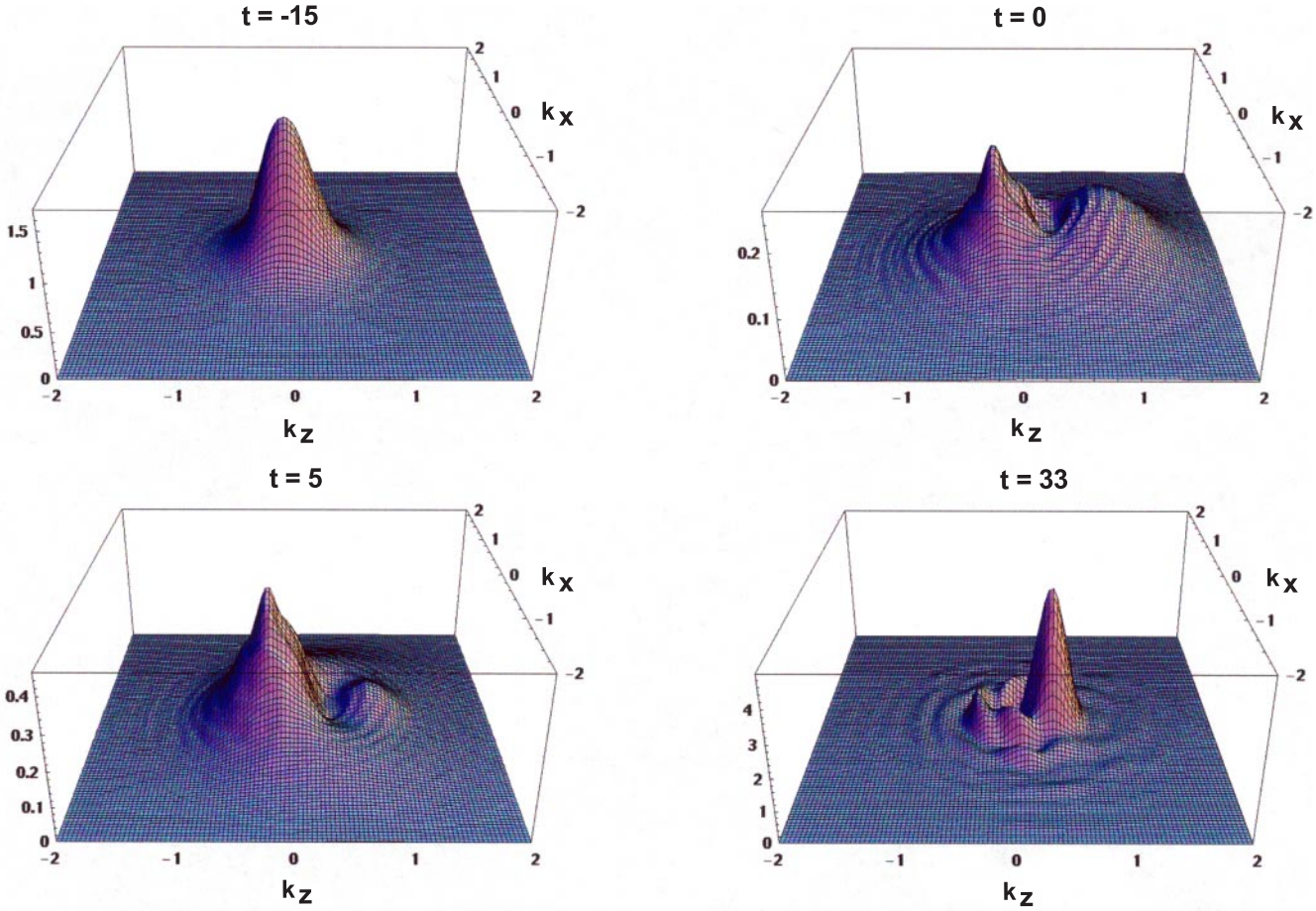

Fig. 1. Time evolution of the momentum space probability density $\psi^\dagger\psi$ for an electron initially bound in the $1s$-state of the uranium target for a central Au^{79+}+ U^{91+} collision at 100 MeV/u. The units of length and time are $\lambda_C = \hbar/(mc) \simeq 386.16$ fm and $\tau_C = \lambda_C/c \simeq 1.29 \times 10^{-21}$ s, respectively. Note the difference in scale for the vertical axis.

of 0.01. Furthermore, the momentum-space wave function $\psi(\mathbf{k}, t)$ is defined in spherical coordinates k, ϑ and φ on a three-dimensional lattice with typically $(64 \times 35 \times 21)$ grid points. While the angular grid points have an equidistant distribution, the radial momentum grid points are distributed logarithmically. Electrons with high momenta are excited in strong-field conditions such that we found it necessary to incorporate momenta up to 10 mc. Furthermore, the $\psi(\mathbf{k}', t)$-values required for the $\mathbf{k}'$-integration of the right hand side of equation (1) are obtained by three-dimensional interpolation, and the integration volume is sliced into cells which are integrated independently using Gauss-Legendre quadrature techniques. Here, the number of grid points is varied in order to obtain an accurate error control.

3 Results and conclusions

We apply this method to a head-on collision between a bare Au^{79+} projectile ion and a hydrogen-like uranium target at an energy of 100 MeV/u. The initial time for the numerical integration is set to $t_i = -92$ corresponding to a projectile-target distance of about 25 K-shell radii of the uranium target. A change of the initial time value t_i to earlier times does not change the present results.

In Figure 1 we show the time evolution of the momentum space probability density $\psi^\dagger(\mathbf{k}, t)\psi(\mathbf{k}, t)$ corresponding to an electron initially bound in the $1s$-state of the uranium target. The initial state wave function is normalized to unity, and by verifying directly that the norm of the time evolved state remains stable at each time step we have a good control of the numerical accuracy. The Au^{79+} projectile ion is approaching the target from negative z values, and $t = 0$ corresponds to the point of closest approach of the collision partners. Note the difference in scale on the vertical axis in Figure 1. One can see in Figure 1 that the probability density associated with the active electron remains localized around the origin as the collision evolves in time. At large negative times the density distribution is very similar to that of the initial $1s$-state. However, as the projectile approaches the target, the electron density shifts toward negative values of k_z reflecting an acceleration of the electron toward the incoming projectile ion. At the time of closest approach, $t = 0$, one finds a global maximum at $k_z = -0.3$. Furthermore, while an important part of the probability density is located around the local maximum at $k_z \simeq 0.7$, we observe that

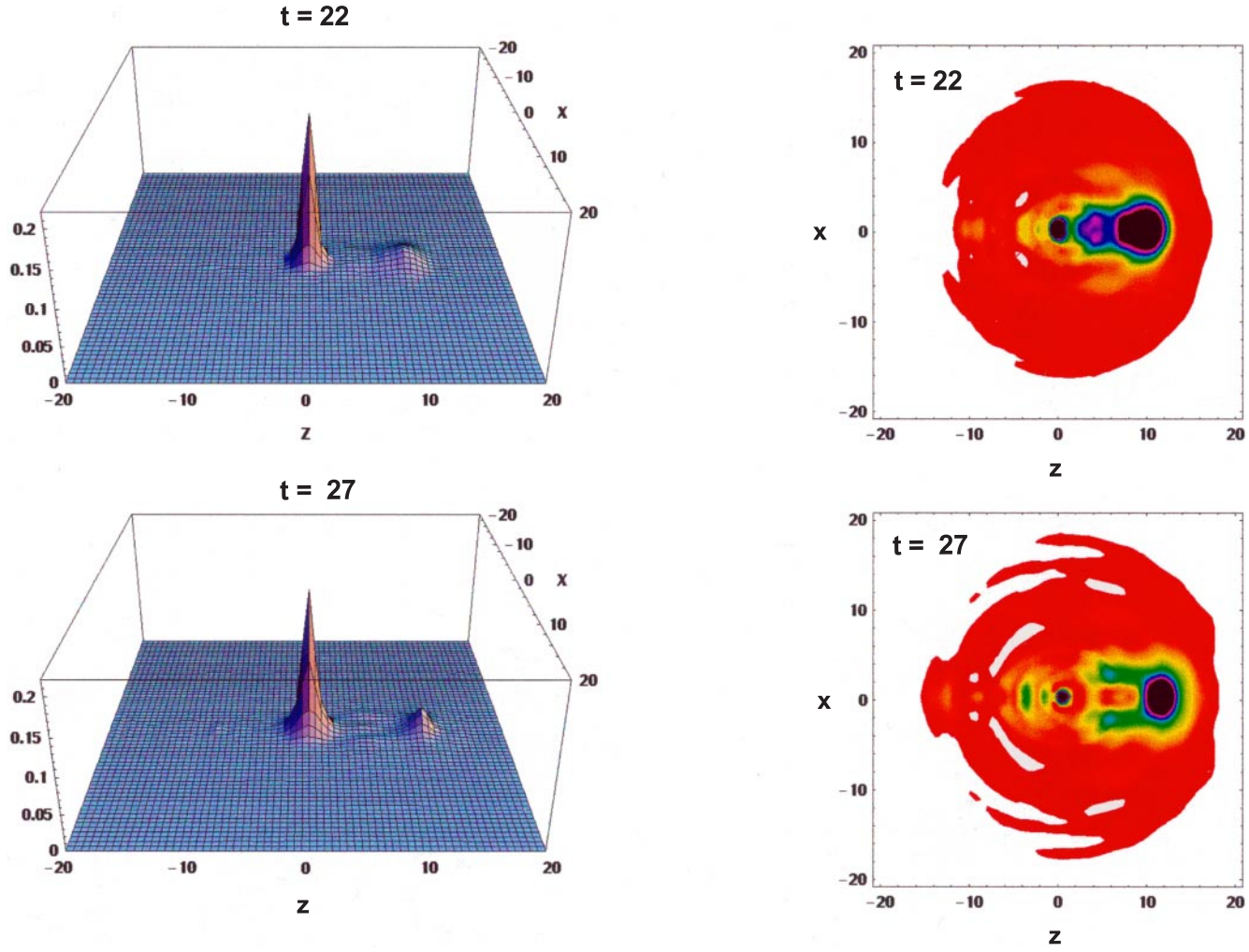

Fig. 2. Time evolution of the configuration space probability density $\Psi^\dagger\Psi$ for the same collision system as in Figure 1. In the contour diagrams shown on the right the projectile is moving from left to right and the target is located at the origin $x = z = 0$. Contributions corresponding to electronic transitions to the target K-shell are coherently subtracted in the contour plots. At $t = 27$ we note a strong local maximum at the position of the moving projectile ion, *i.e.* at $x = 0$ and $z \simeq 11$. This peak is interpreted as charge exchange between bound states and corresponds to transitions from the target $1s$ to the projectile bound states. In addition, there are two distributions peaking around $x = \pm 2.5$ and $z = 5$ that move symmetrically and roughly perpendicular with respect to the beam direction.

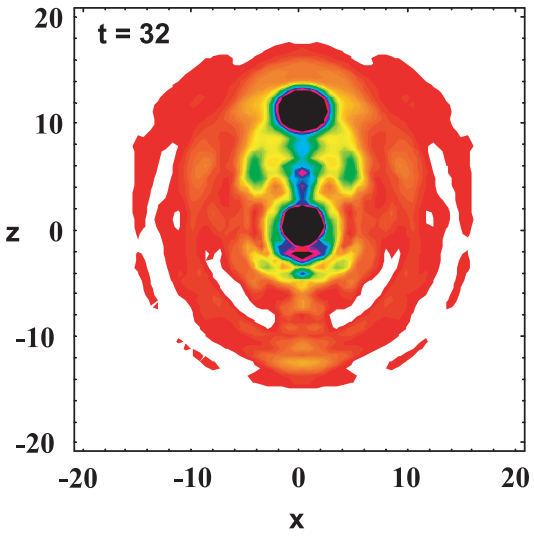

Fig. 3. Contour diagram associated with the complete configuration space probability density $\Psi^\dagger\Psi$ at $t = 32$ for the same collision system as in Figure 1. The projectile is moving from bottom to top and the target is located at the origin. The two symmetric distributions ("transverse peaks") with velocity components $v_x \simeq 0.5$ and $v_z \simeq 0.2$ are located around $x = \pm 5$ and $z = 6$.

high momenta are excited due to the strong transient field associated with the moving projectile. At times following the closest approach ($t = 5$) the density is partially flowing back towards the origin. At later times (see for example $t = 33$) a part of the probability density rebuilds a global maximum around the k_z-axis at $k_z \simeq 0.4$. This value of the momentum corresponds to that of an electron moving with the same velocity as the projectile. It can be understood as the transfer of the electron from the uranium target to the Au^{79+} projectile. Note that contributions associated with the initial $1s$-state and electron transitions to the first excited target states are highly localized in coordinate space such that a sharp maximum of the coordinate space probability distribution $\Psi^\dagger(\mathbf{r},t)\Psi(\mathbf{r},t)$ is to be expected at the origin $x = z = 0$. However, in momentum space this narrow peak containing quite high momentum components of the complete time dependent wave function spreads over a large portion of the k_xk_z-plane and the momentum space distribution $\psi^\dagger(\mathbf{k},t)\psi(\mathbf{k},t)$ is dominated by structures associated with electron transitions from the target ground state to projectile bound states, continuum states, and highly excited target states. These main structures including their tails also determine the main behavior of the final state probability distribution in momentum space around the origin at $k_x = k_z = 0$ where no peak is visible. This reflects the fact that highly localized structures and distributions in coordinate space are poorly localized in momentum space where they spread over the entire space and *vice versa*.

Additional insight into the collision dynamics is obtained by considering the time evolution of the probability density in coordinate space. The momentum-space wave function $\psi(\mathbf{k},t)$ obtained from the numerical solution of equation (1) is transformed to the **r**-space using accurate Fast Fourier Transform techniques in three dimensions yielding the coordinate-space wave function $\Psi(\mathbf{r},t)$. In Figure 2 we display snapshots of the electron probability density $\Psi^\dagger(\mathbf{r},t)\Psi(\mathbf{r},t)$ in coordinate space at two different times for the same collision system as in Figure 1. Here the projectile is approaching the target from negative z-values, and the target is located at the origin $x = z = 0$ of the scattering plane. Therefore, target-centered electron emission would appear centered around the origin while electrons captured to bound or continuum states of the projectile would be located around $x = 0$ and $z = vt$. At $t = 27$ the configuration-space probability density has its global maximum around the target nucleus. This narrow peak is associated with electronic excitations to the target bound states. An additional local maximum is clearly seen at the position of the moving projectile ion, *i.e.* at $vt = 0.4 \times 27 \simeq 11$. While this peak is interpreted as charge exchange from the target $1s$ to the projectile bound states, it also shows that the collision dynamics spreads proportionally with the time t.

In order to unravel the specific features of the different excitation mechanisms, in the contour plots shown in Figure 2 we eliminated contributions associated with transitions to the target K-shell which is the dominant reaction channel as can be seen in the three-dimensional plots in Figure 2. This is achieved by the coherent subtraction of the target $1s$-state, weighted by the complex-valued $1s$-transition amplitude, from the complete time-evolved wave function. Here, the $1s$-transition amplitude is given by the projection of the time-evolved state on the target $1s$-state. Our results show that for large positive times a large part of the electron density is associated with target-centered electron emission in the form of a s-wave spreading over the entire lattice in configuration space. In addition, from the contour plots displayed in Figure 2 we observe that electron emission in the forward direction extends up to values $z \simeq 16$ and $z \simeq 19$ for $t = 22$ and $t = 27$, respectively. This behavior is consistent with the distribution of binary-encounter electrons (BEE) peaking at an electron velocity $V_{\mathrm{BEE}} = 2vc/(c^2 + v^2) \simeq 0.7c$. Note that from relativistic two-body collision dynamics for heavy-particle impact on a free electron, the Lorentz factor Γ_{BEE} of the recoiling electron is $\Gamma_{\mathrm{BEE}} = 2\gamma^2 - 1$ corresponding to the BEE peak. Furthermore, the distribution of electrons moving with the projectile velocity v is seen to be much wider in configuration space as compared to the one in momentum space. This indicates that in addition to the cusp peak associated with electron capture to the projectile continuum the relative importance of electron transfer to excited projectile bound states is important at the collision energies considered here.

Of particular interest are additional structures appearing in the contour plots of Figure 2 in the region between the target and the projectile. In addition to the local maxima at the origin $x = z = 0$ and $x = 0, z = vt$ associated with target and projectile, respectively, it is seen that at $t = 22$ the probability density displays a third local maximum which is located around $x = 0$ and $z \simeq 4$. However, as it is evident from the lower density contour plot, this maximum separates into two distinctly different maxima moving symmetrically and roughly perpendicular with respect to the beam direction. We interpret this as an additional ionization mechanism in which electrons are emitted with relatively high transverse and low longitudinal velocities with respect to the projectile trajectory. Thus, at $t = 27$ we find two symmetric distributions peaking around $x = \pm 2.5$ and $z = 5$ from which the velocity components of the associated electrons are estimated as $v_x \simeq 0.5$ and $v_z \simeq 0.2$. Note that in contrast to the saddle point emission, these electrons have velocities which are higher than that of the projectile ion which is approximately 0.4.

In Figure 3 we display the emission characteristics of these symmetric distributions at a later time, $t = 32$, corresponding to an internuclear separation of $9a_{\mathrm{K}}$, where $a_{\mathrm{K}} = a_0/Z \simeq 576$ fm is the nonrelativistic uranium K-shell radius (with $a_0 = \lambda_{\mathrm{c}}/\alpha \simeq 0.53 \times 10^{-10}$ m being the Bohr radius of hydrogen). Here it is clearly seen that the transverse distributions peak around $x = \pm 5$ and $z = 6$ which is consistent with the previous velocity determination. For getting an estimate on the importance of the reaction channel associated with this unexpected fast electron emission in the transverse direction we projected the time evolved wave function on wave packets describing free

electrons. Assuming the velocities of these electrons given by the velocity components of the transverse peaks we arrive at a value around one percent. We note however, that this result still shows a weak dependence on time which indicates that the asymptotic region belonging to this particular channel is not completely reached. Remembering also that the assumptions we made to extract this result are rather crude, this value is to be regarded as a quite rough estimate. For a rigorous prediction of the magnitude of the new ionization mechanism more detailed studies are needed. In particular, future more comprehensive investigations will have to incorporate the complete range of impact parameters for calculating the complete impact parameter dependent probability $P(b)$ and larger time intervals. We note that the considered case $b = 0$ carries zero weight in the total cross section which is proportional to $\int_0^\infty \mathrm{d}b\, bP(b)$.

Furthermore, from the snapshots of the probability density at different times one may directly visualize and study in real time the dynamic evolution of the collision system by means of a computer animation. We find that the electrons ejected as a result of this new mechanism are emitted from the internuclear region after the projectile passes the target at relatively large positive times, *i.e.* $t > 17$. As the projectile passes the target a very strong combined field is produced leading to a high acceleration of the active electron which initially follows the projectile ion, scatters several times in the two-center electromagnetic field associated with the collision partners, and at later positive times, as the system relaxes, is ejected from the internuclear region preferentially in the transverse direction. Note that at large times, the magnitude of the two-center potential, at points located approximately halfway between the collision partners, is substantially lowered in the transverse direction than in the longitudinal one.

As mentioned earlier, recent measurements of electron velocity spectra for intermediate energy atomic collisions involving 45 MeV/u Ni^{28+} projectile ions impinging on various solid state targets [11] exhibit an unexpectedly large number of very fast electrons. For heavy Au targets, an important number of electrons with velocities considerable *higher* than the projectile velocity are found to be present in the tail of the spectra. A multiple scattering mechanism, also referred to as "Fermi-shuttle" mechanism, where the active electron scatters several times between projectile and target, was proposed to explain the fast electron emission in ion-atom collisions [11]. Our present investigation extends the results on this "Fermi-shuttle" electron acceleration into the nonperturbative regime associated with highly-charged ions as heavy as uranium and provides additional insight into the dynamics of fast electron emission in relativistic heavy-ion collisions.

In conclusion, by analyzing the calculated momentum- and configuration-space distributions of emitted electrons in encounters between 100 MeV/u Au^{79+} projectile ions and hydrogen-like uranium targets we unravel the different mechanisms associated with elementary atomic processes which occur in relativistic heavy-ion collisions. In particular, we identify a new ionization mechanism in which unexpected fast electrons are emitted from the internuclear region preferentially in the transverse direction. Distinctly different from the saddle point promotion known from slow ion-atom encounters this mechanism is associated with electrons having high acceleration components perpendicular to the beam trajectory resulting in an electron velocity which is higher than that of the projectile. Impact parameter dependent measurements of momentum and angular distributions of emitted electrons for heavy-ion collisions in the energy regime studied in the present work are planned in the near future at GSI-Darmstadt [23]. We expect these differential cross-section measurements of emitted electrons to display the features described here. The present nonperturbative approach is quite flexible in nature and may be applied to other challenging time dependent problems such as the motion and the behavior of electrons in super-intense short-pulsed laser fields, showing significant promise for further investigations of the dynamics in extreme and unusual conditions.

We would like to thank Horst-Schmidt Böcking, G. Lanzano, and H. Rothard for useful discussions on the Fermi-shuttle mechanism and for important discussions of their experimental results before publication. This work was supported by the Office of Science, Office of Basic Energy Sciences, of the U.S. Department of Energy (DOE) under contract No. DE-AC03-76SF00098 through Lawrence Berkeley National Laboratory's Laboratory Directed Research and Development (LDRD). D.C.I. was supported in part by the Deutsche Forschungsgemeinschaft (DFG) through a Heisenberg Fellowship.

References

1. J. Eichler, W. Meyerhof, *Relativistic Atomic Collisions* (Academic Press, San Diego, 1995).
2. U. Becker, N. Grün, W. Scheid, J. Phys. B **18**, 4589 (1985).
3. *Physics of Strong Fields*, edited by W. Greiner, NATO ASI Ser. B (Plenum, New York, 1987), Vol. 153; see section written by U. Becker, N. Grün, K. Momberger, W. Scheid, p. 609.
4. E.A. Solov'ev, Phys. Rev. A **42**, 1331 (1990).
5. S.Yu. Ovchinnikov, J. Macek, Phys. Rev. Lett. **75**, 2474 (1995).
6. M. Pieksma, S.Yu. Ovchinnikov, J. Phys. B **27**, 4573 (1994).
7. M. Pieksma, S.Yu. Ovchinnikov, J. van Eck, W.B. Westerveld, A. Niehaus, Phys. Rev. Lett. **73**, 46 (1994).
8. S.D. Kravis, M. Abdallah, C.L. Cocke, C.D. Lin, M. Stöckli, B. Walch, Y.D. Wang, R.E. Olson, V.D. Rodriguez, W. Wu, M. Pieksma, N. Watanabe, Phys. Rev. A **54**, 1394 (1996).
9. J. Ullrich, R. Moshammer, R. Dörner, O. Jagutzki, V. Mergel, H. Schmidt-Böcking, J. Spielberger, Top. Rev. J. Phys. B **30**, 2917 (1997).
10. R. Dörner, H. Kehmliche, M.H. Prior, C.L. Cocke, J.A. Gary, R.E. Olson, V. Mergel, J. Ullrich, H. Schmidt-Böcking, Phys. Rev. Lett. **77**, 4520 (1996).
11. G. Lanzano, E. De Filippo, D. Mahboub, H. Rothard, S. Aiello, A. Anzalone, S. Cavallaro, A. Elanique, E. Geraci,

M. Geraci, F. Giustolisi, A. Pagano, G. Politi, Phys. Rev. Lett. **83**, 4520 (1999); see also Phys. Rev. A **63**, 032702 (2001).
12. E. Fermi, Phys. Rev. **75**, 1169 (1949).
13. P.L. Biermann, J. Phys. G **23**, 1 (1997).
14. C. Carraro, B.Q. Chen, S. Schramm, S. Koonin, Phys. Rev. A **42**, 1379 (1990).
15. M. Hautala, Z. Pan, P. Siegmund, Phys. Rev. A **44**, 7428 (1991).
16. S. Suarez, G. Bernard, P. Focke, W. Meckbach, M. Tobish, M. Jung, H. Rothard, M. Schosnig, R. Maier, A. Clouvas, K.O. Groeneveld, Nucl. Instrum. Meth. Phys. Res. B **86**, 197 (1994).
17. K. Momberger, A. Belkacem, A.H. Sørensen, Phys. Rev. A **53**, 1605 (1996).
18. D.C. Ionescu, A. Belkacem, Phys. Scripta **T80**, 128 (1999).
19. D.R. Schultz, M.R. Strayer, J.C. Wells, Phys. Rev. Lett. **82**, 3976 (1999).
20. E.Y. Sidky, C.D. Lin, Phys. Rev. A **60**, 377 (1999).
21. J. Eichler, Phys. Rep. **193**, 165 (1990).
22. Th. Stöhlker, D.C. Ionescu, P. Rymuza, F. Bosch, H. Geissel, C. Kozhuharov, T. Ludziejewski, P.H. Mokler, C. Scheidenberger, Z. Stachura, A. Warczak, R.W. Dunford, Phys. Rev. A **57**, 845 (1998); see also Phys. Lett. A **238**, 43 (1998).
23. Th. Stöhlker, private communication.